JOURNAL OF GEOPHYSICAL RESEARCH, VOL. 104, NO. D17, PAGES 21,733–21,749, SEPTEMBER 20, 1999

One-dimensional modeling of sulfur species during the First Aerosol Characterization Experiment (ACE 1) Lagrangian B

Céline Mari,[1] Karsten Suhre,[1] Robert Rosset,[1] Timothy S. Bates,[2]
Barry J. Huebert,[3] Alan R. Bandy,[4] Donald C. Thornton,[4] and Steve Businger[5]

Abstract. A one-dimensional Lagrangian model is used to simulate vertical profiles and temporal evolution of dimethylsulfide (DMS), sulfur dioxide (SO_2), aerosol methane sulfonate, and non-sea-salt sulfate (nss sulfate) that were measured during the three flights of the second First Aerosol Characterization Experiment (ACE 1) Lagrangian (Lagrangian B) experiment. Entrainment rate, mixing heights, and cloud occurrence are calculated prognostically in this type of model. The model is forced by geostrophic winds and large scale subsidence from European Centre for Medium-Range Weather Forecasts (ECMWF) analysis and sea surface temperature measured on board Research Vessel *Discoverer*. Gas phase oxidation and heterogeneous oxidation of SO_2 to nss sulfate in clouds and sea-salt particles are considered. The evolution of dynamical variables in the column is found to be well reproduced by the model. The model captures 82% of the variance of observed DMS assuming OH is the only oxidant and a DMS flux term calculated from *Liss and Merlivat* [1986] parameterization and seawater DMS concentrations measured aboard R/V *Discoverer*. However, uncertainties in DMS oxidation rates and regional seawater concentrations are too great to identify a best fit wind speed-transfer velocity relationship. SO_2 mixing ratios are correctly represented in the model (least squares correlation coefficient r^2= 75%) using a DMS to SO_2 conversion efficiency of about 70%. Oxidation of SO_2 in sea-salt particle appears to be a dominant process and controls SO_2 lifetime during the Lagrangian B at least in the well mixed lower layer. Removing heterogeneous loss of SO_2 in sea salt significantly deteriorates the simulation (r^2= 50%). Under cloudy conditions, heterogeneous loss in cloud droplets and in sea-salt particles are competitive (relative rates are 35% and 41%, respectively, during flight 26). Model-generated aerosol methane sulfonate mixing ratios agree with the observations (r^2= 62.5%) when high branching ratio for an addition oxidation pathway is used. The model estimates nss sulfate mixing ratios with little bias (median simulated-to-observed concentration ratio 1.03 and slope of the regression line 0.7) but captures only one third of the observed variance of nss sulfate. Part of the discrepancy could be due to the assumption of a decrease of nss sulfate mixing ratios with altitude in the model, whereas observations revealed high concentrations at 4500 m during the last two flights suggesting that horizontal transport could be more important than vertical mixing in this region. Nss sulfate is found to be produced photochemically under non cloudy, low wind speed conditions encountered during the first flight. During the last two flights, nss sulfate is produced mainly by oxidation in cloud droplets (48% during flight 25 and 69% during flight 26) and sea-salt particles (50% during flight 25 and 22% during flight 26).

[1] Laboratoire d'Aérologie, UMR CNRS/Université Paul Sabatier, Toulouse, France.

[2] Pacific Marine Environmental Laboratory, NOAA, Seattle, Washington.

[3] Departement of Oceanography, University of Hawaii, Honolulu.

[4] Department of Chemistry, Drexel University, Philadelphia, Pennsylvania.

[5] Departement of Meteorology, University of Hawaii, Honolulu.

Paper number 1999JD900022.
0148-0227/99/1999JD900022$09.00

1. Introduction

The southern hemisphere First Aerosol Characterization Experiment (ACE 1) was focused on the physical and chemical processes controlling the formation and fate of remote marine aerosols in air masses that were not influenced by anthropogenic sources [*Bates et al.*, 1998a]. During ACE-1, a lagrangian study (Lagrangian B) was conducted during which an air mass was tagged and sampled over a 29 hour period. This experiment was designed to capture the vertical characterization of the lower troposphere without the confounding effect of air mass changes [*Huebert et al.*, 1996].

This experimental approach was motivated by the difficulties in deriving surface fluxes and atmospheric reaction rates from Eulerian observations which are influenced by advection processes and horizontal gradients in both atmosphere and ocean. This is particularly true for the sulfur budget as large uncertainties still prevail on both sea-air emission and oxidation rates of dimethylsulfide (DMS), which is thought to be the primary gaseous precursor of nss sulfate aerosols in the remote marine atmosphere. During Lagrangian B, vertical distributions of dimethyl sulfide (DMS), sulfur dioxide (SO_2), aerosol methane sulfonate (MS), and non-sea-salt sulfate (nss sulfate) were measured simultaneously during three flights of the National Center of Atmospheric Research (NCAR)/C130 aircraft, offering tremendous potential for studying these atmospheric sulfur species and chemical budgets.

In this work, the results of these measurements are investigated with a one-dimensional (1-D) lagrangian model [*Suhre et al.*, 1998] coupled "on-line" with sulfur chemistry, including heterogeneous effects of clouds and sea-salt particles. The model is used to simulate the vertical distribution and temporal evolution of DMS and its oxidation products (SO_2, MS, and nss sulfate). It provides a unique and powerful way to investigate the complex interplay between the atmospheric processes involved in sulfur budget during the lagrangian experiment. A particular effort has been made to use measurements not only for point-by-point comparison with the model outputs but also to constrain as much as possible free parameters by their observed values. This approach ensures that the model reflects as closely as possible the Lagrangian B experimental conditions.

2. Model Description

2.1. Dynamics

The dynamics of the model used to perform the simulation of the Lagrangian B has been documented in detail by *Suhre et al.* [1998] for the same experiment. Prognostic variables are the vertical profiles of latitudinal and longitudinal wind components, potential temperature, water vapor, cloud and rain mixing ratios, the mixing ratio of the different chemical species, and turbulent kinetic energy. Our 1-D model is a Lagrangian model where geostrophic wind, synoptic scale vertical velocity, and the sea surface temperature are varied following the Lagrangian B trajectory. These forcing terms are extracted from European Centre for Medium-Range Weather Forecasts (ECMWF) analysis except sea surface temperature (SST) which was measured on board the R/V *Discoverer*. In our previous study [*Suhre et al.*, 1998], the objective was to show that the model was able to reproduce the time evolution and the vertical distribution of the observed dynamical variables and chemical species, when forced only with ECMWF analysis. The purpose of this paper is to study sulfur species evolution and budget during Lagrangian B. Thus our approach here is to improve the dynamical simulation by fine-tuning the forcings of the dynamical variables without answering the question of why these forcings need to be modified.

In particular, the simulation has been improved by taking into account the pressure drop at the end of the Lagrangian from 1012 hPa on December 7 1800 UTC to 997 hPa on December 9 0000 UTC. This induces higher cloud water mixing ratio for the upper layer cloud during flight 26 in agreement with the data. Figure 1 shows the cloud water mixing ratios for nine aircraft soundings made during Lagrangian B. A good simulation of cloud water mixing ratio is essential for the simulation of heterogeneous loss of SO_2 in cloud droplets. ECMWF-analyzed geostrophic wind used to force the model has been reduced by 3 m/s during flight 26, correcting the tendancy of ECMWF analysis to overestimate wind speed at the end of the experiment. This is of particular importance as wind speed controls both the sea-air flux of DMS and the production of sea salt at the surface. Finally, synoptic-scale vertical subsidence has been adjusted to reduce the discrepancies between simulated and observed vertical profiles of potential temperature during flight 26. This adjustement gives us even more confidence on the entrainment which is calculated prognostically in the model as the difference between the turbulent boundary layer growth and the imposed synoptic-scale subsidence or ascent.

2.2. Chemistry

Six species are included in our simulation: (1) DMS emitted from the ocean, (2) SO_2 produced by oxidation of DMS, (3) secondary submicronic aerosol nss sulfate in dry air ($SO_4^=$a) produced by oxidation of SO_2 by OH or oxidation of SO_2 in sea-salt particles, (4) secondary nss sulfate in cloud water ($SO_4^=$c) produced by heterogeneous oxidation of SO_2 in cloud droplets or by the uptake of dry air nss sulfate when clouds form, (5) submicronic aerosol methane sulfonate (MSa) in dry air produced by the oxidation of DMS, and (6) methane sulfonate in cloud water (MSc) produced by the uptake of dry air MS during cloud condensation. Each constituent in each microphysical reservoir (e.g., water vapor, cloud water) is represented by a differential equation for mass continuity. The source and sink terms in the equations represent either the transfer ($Q_{c_i}^{\text{trans}}$) of a constituent from one microphysical reservoir to another (e.g., transfer of cloud water nss sulfate to dry air nss sulfate by evaporation) or a chemical reaction ($Q_{c_i}^{\text{chem}}$) (e.g., oxidation of SO_2 in cloud water nss sulfate). These equations are of the form

$$\frac{\partial c_i}{\partial t} = \frac{\partial}{\partial z}\left(K_h \frac{\partial c_i}{\partial z}\right) - w_{ls}\frac{\partial c_i}{\partial z} + Q_{c_i}^{\text{chem}} + Q_{c_i}^{\text{trans}}$$

K_h is the turbulent mixing coefficient for heat calculated nonlocally in the model as a function of stability, and w_{ls} is the synoptic scale vertical velocity adjusted from ECMWF analysis. The various fields and their sources and sinks are shown schematically in Figure 2.

2.2.1. Gaseous phase chemistry. Large uncertainties still prevail about the DMS oxidation rates and products. A number of simplified schemes have been proposed using branching ratios to predict the oxidation products of DMS [*Kreidenweis et al.*, 1991; *Benkovitz et al.*, 1994; *Pham et al.*, 1995; *Chin et al.*, 1996]. These authors argued that uncertainties associated with other processes in global atmo-

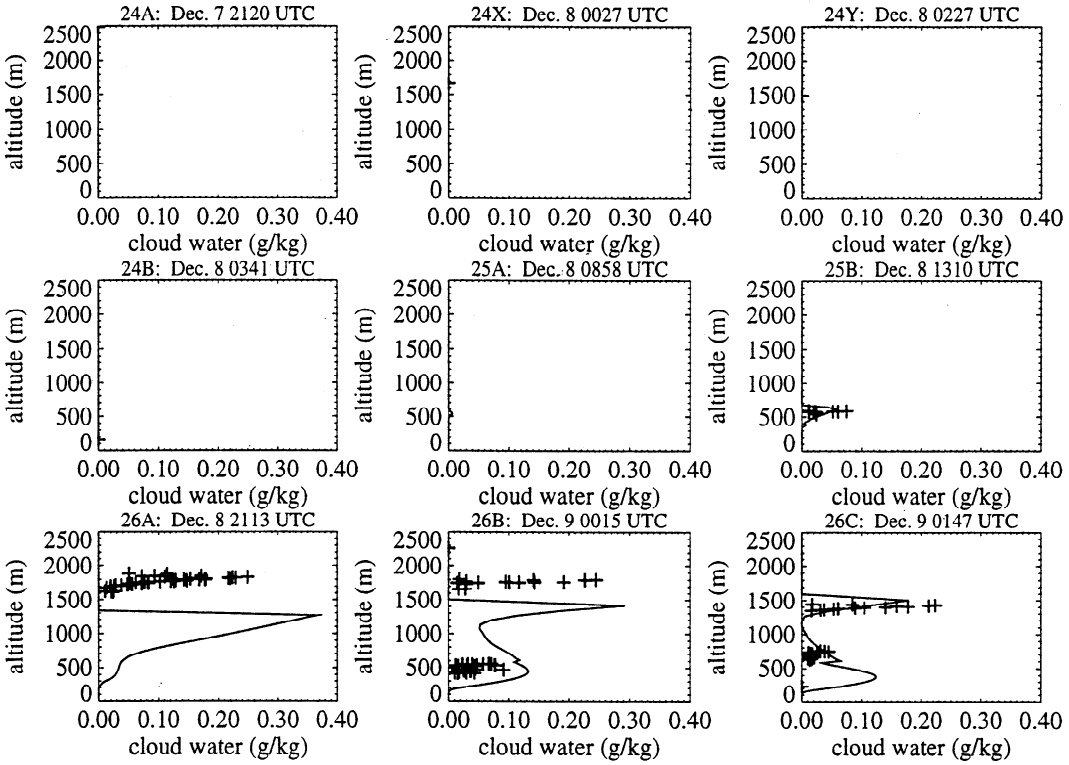

Figure 1. Cloud water mixing ratio (in g/kg) during the nine aircraft soundings of Lagrangian B: data (crosses) and simulation (solid line). Note that the observations are biased by the fact that the aircraft tried to avoid clouds as much as possible.

spheric chemistry and transport models dominate the uncertainties of sulfate prediction and that those associated with DMS oxidation mechanism are minor. We choose to adopt the same parameterized oxidation scheme in the 1-D model with a branching ratio for the addition oxidation pathway (α) of 0.6 in the baseline scenario. Table 1 presents the reaction rate constants for the addition and abstraction pathways as a function of temperature using expressions derived by *Hynes et al.* [1986]. Note that the temperature during the field experiment was generally below 283 K, favoring the addition pathway. Our aim is to determine to what degree such simplified approach is appropriate to represent SO_2, MS, and nss sulfate mixing ratios using higher vertical and temporal resolutions than global scale models. In addition, the 1-D lagrangian model allows to test this simplified chemical scheme with reduced uncertainties in the transport of simulated species (Lagrangian frame) and microphysical fields (cloud water is a prognostic variable in this model, whereas it is usually given by climatological data in global models or arbitrarily imposed in box models). An additional reaction is also implemented in the model for oxidation of DMS to perform sensitivity study as proposed by *Chin et al.* [1996]. This reaction has been proposed by several authors [*Cooper and Saltzmann*, 1993; *Jacob et al.*, 1995; *Suhre et al.*, 1995; *Yvon et al.*, 1996] to explain the observed concentrations of DMS and its products. The need of this reaction suggests that there may be an important unknown DMS oxidant or oxidation pathway. This reaction, however, is not required systematically, and some studies have shown that the oxidation by OH could be sufficient to explain observed DMS and products levels [*Bandy et al.*, 1996; *Mari et al.*, 1998; *Davis et al.*, 1998].

2.2.2. Aqueous phase chemistry in clouds. SO_2 is rapidly oxidized to nss sulfate in cloud droplets through reaction with hydrogen peroxide [*Pandis and Seinfeld*, 1989]. Oxidation of SO_2 with O_3 proceeds only if there is any residual SO_2 after the reaction with H_2O_2. H_2O_2 and O_3 are initially specified in the model as gas-phase fields. The gas

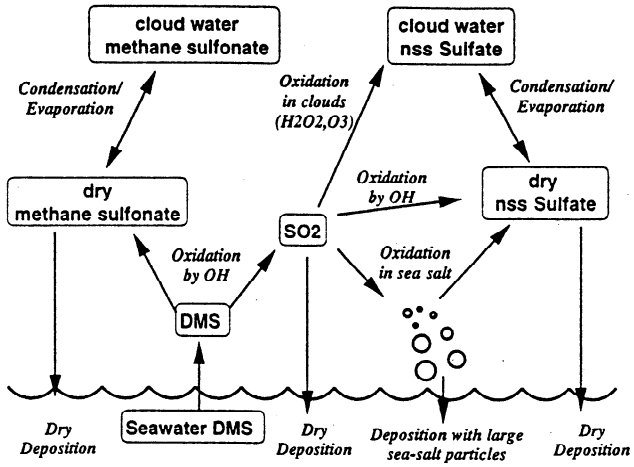

Figure 2. Schematic showing the various sulfur fields (boxes) and the main transfer and chemical processes (arrows) included in the model.

Table 1. Chemical Mechanism in the Model

Reaction	Rate Coefficient, $cm^3\ mol^{-1}\ s^{-1}$	Note
$DMS + OH \longrightarrow SO_2$	$k_{abs} = 9.6 \times 10^{-12} \exp(-234/T)$	1
$DMS + OH \longrightarrow \alpha SO_2 + (1-\alpha)MSa$	$k_{add} = k_{obs} - k_{abs}$	1
	with $k_{obs} = \frac{T \exp(-234/T) + 8.46 \times 10^{-10} \exp(7230/T) + 2.68 \times 10^{-10} \exp(7810/T)}{1.04 \times 10^{11} T + 88.1 \exp(7460/T)}$	
$DMS + X \longrightarrow SO_2$	k_{obs}	2
X is an additional oxidant		
$SO_2 \longrightarrow$ nss sulfate	$k_{SO_2} = \frac{k_0 M}{1 + k_0 \frac{M}{k_\infty}} F_c^{(1 + [\log(k_0 \frac{M}{k_\infty}]^2)^{-1}}$	3
	with $k_0 = 4.0 \times 10^{-31} (T/300)^{-3.3}$,	
	$k_\infty = 2.0 \times 10^{-12}$	
	and $F_c = 0.45$	

Notes: (1) k_{abs} and k_{obs} from *Hynes* [1986], (2) *Chin et al.* [1996], and (3) *Atkinson et al.* [1992]

are allowed to absorb into liquid hydrometeors. H_2O_2 is depleted by reaction with aqueous SO_2, whereas O_3 remains unchanged. The equilibrium partitioning of H_2O_2, SO_2, and O_3 between the gas and liquid phase are assumed to follow Henry's law (Table 2). The effective Henry's law coefficients are calculated assuming a fixed pH for cloud water of 4.5.

2.2.3. Emissions. The DMS emission flux in the reference case is deduced from *Liss and Merlivat* [1986] parameterization of exchange velocity at the sea surface and seawater concentrations measured on board the R/V *Discoverer* [*Bates et al.*, 1998b] (Figures 3a and 3b). The flux calculated using *Wanninkhof* [1992] wind speed transfer velocity relationship is also available in the model, and sensitivity to this parameterization will be discussed.

2.2.4. Dry deposition. Dry deposition velocities of SO_2 and submicronic particulate nss sulfate and MS are calculated as described by *Wesely* [1989]. A series resistance model approach is used, with deposition velocity being inversely proportional to the sum of three resistance terms: aerodynamic resistance, quasi-laminar layer resistance, and a canopy resistance. Canopy resistance can be neglected over the ocean for SO_2 and is taken equal to zero for particles. Quasi-laminar layer resistance is calculated following *Wesely* [1989]. Aerodynamic resistance is calculated as a function of wind, atmospheric stability, and surface roughness in the model. For submicronic particulate nss sulfate and MS, deposition velocity includes the effect of settling velocity [*Seinfeld and Pandis*, 1998]. Dry deposition velocities obtained along the Lagrangian B trajectory vary from 0.3 to 1.3 cm/s for SO_2 and 0.005 to 0.012 cm/s for submicronic particulate nss sulfate and MS (Figure 3c). The values for nss sulfate and MS lie in the lower range of the values found in the literature which vary from 0.01 to 0.7 cm/s [*Chin et al.*, 1996; *Pham et al.*, 1995; *Benkovitz et al.*, 1994; *Langner and Rodhe*, 1991; *Capaldo and Pandis*, 1997].

2.2.5. Parameterization of sea-salt particles. Reactions in sea-salt particles also convert SO_2 to sulfate, but in this case the dominant oxidant is ozone [*Sievering et al.*, 1992].

Table 2. Henry's Law Coefficients for H_2O_2, O_3 and SO_2, Dissociation Rates of SO_2 , and Oxidation Rates of SO_2 to nss sulfate in Water

			$K(T=298)^a$, $M\ atm^{-1}$	$\Delta H_{298}/R$ (K)	Note
$H_2O_2(g)$	$\leftrightarrow$	$H_2O_2(aq)$	7.4×10^4	-6600	1
$O3(g)$	$\leftrightarrow$	$O_3(aq)$	1.15×10^{-2}	-2560	2
$SO_2(g)$	$\leftrightarrow$	$SO_2(aq)$	1.23×10^0	-3135	3
$SO_2(aq)$	$\leftrightarrow$	$H^+ + HSO_3^-$	1.7×10^{-2}	-2090	4
HSO_3^-	$\leftrightarrow$	$H^+ + SO_3^=$	6.3×10^{-8}	-1495	3
			Oxidation Rate, mol $L^{-1}\ s^{-1}$		
$SO_2(aq) + H_2O_2(aq)$	$\rightarrow$	$SO_4^=$ c in water	$R_1 = \frac{8 \times 10^4 \exp(-3650(\frac{1}{T} - \frac{1}{298}))}{0.1 + [H^+]}$		5
$SO_3^= + O_3(aq)$	$\rightarrow$	$SO_4^=$ c in water	$R_2 = 4.39 \times 10^{11} \exp(-\frac{4131}{T}) + \frac{2.56 \times 10^3 \exp(-\frac{966}{T})}{[H^+]}$		6

Notes: (1) *Lind et Kok* [1986], (2) *Johnson et Isaksen* [1993], (3) *Hoffmann et Calvert* [1985], (3) *Chameides* [1984], (4) *Martin* [1984], and (5) *Maahs* [1983].

[a] $K(T) = K(T=298) exp\left[\frac{\Delta H_{298}}{R}\left(\frac{1}{298} - \frac{1}{T}\right)\right]$

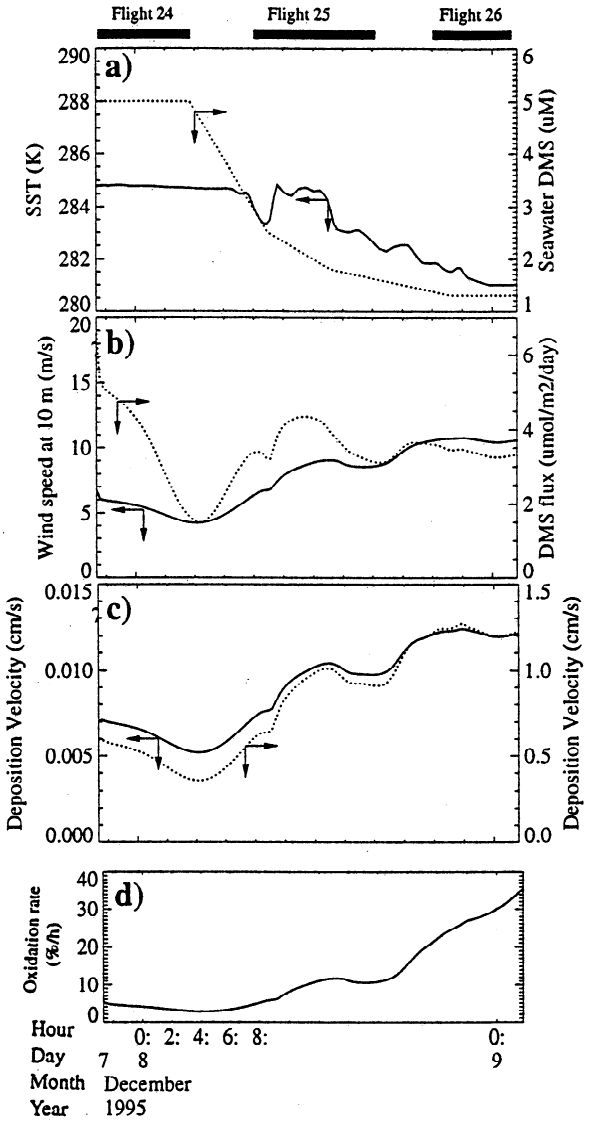

Figure 3. (a) Time series of seawater DMS concentrations in nM (dotted line) and sea surface temperature in K (solid line) measured aboard R/V *Discoverer* and interpolated as a function of time along the Lagrangian B trajectory. Note that seawater DMS concentrations and sea surface temperature were observed aboard R/V *Discoverer* on December 9, as the ship started moving southeast, 1 day after the Lagrangian experiment started. (b) Time series of wind speed at 10 m in m/s (solid line) and DMS sea-air flux in μmol m^{-2} d^{-1} (dotted line) during Lagrangian B. (c) Time series of deposition velocity in cm/s for nss sulfate and MS aerosols (solid line) and SO_2 (dotted line) during Lagrangian B. (d) Time series of SO_2 oxidation rate in sea-salt particles at 10 m in %/h during Lagrangian B.

The ozone reaction is sensitive to pH, and the buffering capacity of sea salt keeps the pH high enough that the ozone reaction can proceed. In this work, pH is fixed to 7.4 which is in the range of commonly assumed values for sea-salt particles [*Winkler*, 1986].

Heterogeneous oxidation of SO_2 in sea-salt particles is treated as a pseudo first-order reaction in the model. The reaction constant k_a is given by the relation

$$\frac{1}{k_a} = \frac{1}{k_{\text{scav}}} + \frac{1}{k_{\text{ox}}}$$

where k_{scav} is the gas-to-particle transfer rate and k_{ox} is the oxidation of dissociated $SO_3^=$ by ozone into the sea-salt particles. These rates are parameterized as a function of the sea-salt distribution, which in turn depends on height, humidity, and aerosol distribution at the surface. This approach has been applied successfully by *Suhre et al.* [1995] in the tropical marine boundary layer to explain the SO_2 levels and evolution.

2.2.5.1. Scavenging in the sea-salt particles. Scavenging rate of SO_2 in sea-salt particles is calculated as a function of the sea-salt particles distribution

$$k_{\text{scav}} = \frac{1}{2}\int \Psi(D) n(D) \frac{\pi}{6} D^3 dD$$

$\Psi(D)$ describes the SO_2 transfer rate into a particle of diameter D and is given by the relation [*Schwartz*, 1986]

$$\Psi(D) = 4\frac{l\bar{v}}{D^2}\frac{1}{1+2\frac{4l}{3\alpha D}}$$

where $\bar{v} = \sqrt{\frac{8RT}{m_{SO_2}\pi}}$ is the mean speed of gas molecules, $l = 0.0665$ μm is the mean free path length, $R = 8.314$ $J\,mol^{-1}\,K^{-1}$, m_{SO_2} is the molecular weight, and $\alpha = 0.1$ is the mass accomodation coefficient. Following *Chameides and Stelson* [1992], we assume a lognormal distribution for the sea-salt aerosols

$$n(D) = \frac{N_o}{\sqrt{2\pi} ln\sigma D} exp\left(-\frac{ln(\frac{D}{D_g})^2}{2ln^2\sigma}\right)$$

where N_o is the total particle number density, D_g is the geometric mean diameter and σ is the dispersion. The parameters of the lognormal distribution used in this study are derived from the number distribution of aerosols measured during ACE 1 aboard R/V *Discoverer* [see *Bates et al.*, 1998b, Figure 3]. A typical mean geometric diameter at 10% RH of 0.54 μm and 2.02 dispersion are used. Sea-salt aerosols in the coarse mode have been found to have a strong exponential dependence on wind speed [*Woodcock*, 1953; *Lowett*, 1978; *Gras and Ayers*, 1983; *de Leeuw*, 1986; *O'Dowd and Smith*, 1993]. Although an exponential dependence explained only 32% of the variance in total number concentration in the coarse mode during ACE 1, the following relationship was deduced from the correlation between wind speed and coarse aerosol number near the surface [*Bates et al.*, 1998b]:

$$N_o = 10^{0.11U}$$

where U is the instantaneous wind speed in m/s and, N_o is given in cubic centimeters.

The vertical profile of sea-salt particles is approximated with an exponential decrease with altitude [*Jaenicke*, 1993; *Kristament et al.*, 1993]:

$$N(z) = N_o exp(-\frac{z}{H})$$

We deduce the scaling height H according to the vertical distributions of sodium and chloride concentrations [*Huebert et al.*, 1998], which are the main constituents of sea salt, observed during the three flight of Lagrangian B (Figure 4). An exponential function is fitted on these measurements giving a scaling height of 500 m.

The mean diameter D_g is parameterized as a function of the relative humidity calculated in the model following the relation of *de Leeuw* [1989]

$$D = D_{\mathrm{dry}} g(S) \quad \text{with} \quad g(S) = 1.2 \exp\left(\frac{0.066S}{1.058 - S}\right)$$

where D_{dry} is the diameter of the dry particle. This relation is valid for relative humidities S between 80 and 99.5%.

2.2.5.2. Oxidation by ozone into the sea-salt particles. Oxidation rate of SO_2 by O_3 is given by the relationship

$$k_{\mathrm{ox}} = \mathrm{Vol}\ R_2\ D_2\ D_1\ [\mathrm{H}^+]^{-2}\ K_{\mathrm{SO}_2}\ K_{\mathrm{O}_3} (RT)^2 [\mathrm{O}_3]$$

where R_2 is the liquid phase reaction constant for $SO_3^=$ oxidation by O_3 [*Maahs*, 1983], Vol denotes the aerosol volume ratio, K_{SO_2} and K_{O_3} are Henry's law constants, and D_1 and D_2 are the dissociation constants for S(IV) (Table 2).

Figure 3d illustrates the variation of the pseudo first-order reaction rate of SO_2 in sea salt near the surface. k_a varies from 5%/h at the beginning of the Lagrangian to 35%/h under strong wind speed conditions during flight 26.

At pH = 7.4, SO_2 removal in sea salt is limited by reaction with O_3. A sensitivity study has been performed with pH fixed to 8. For such high pH, reaction of SO_2 with O_3 is so fast that SO_2 mass tranfer is the rate limiting factor, with rates at the surface about twice the rates obtained with pH = 7.4. The rate-limiting factor then becomes SO_2 mass transfer. However, SO_2 and nss sulfate mixing ratios do not differ from the reference simulation by more than 10%. It is noted that during flight 24, oxidation rate of SO_2 in sea salt and SO_2 mixing ratios are low. Thus even doubling the oxidation rate will not change SO_2 mixing ratios dramatically. During flight 25 and 26, oxidation rate increases with wind speed, but heterogeneous loss in sea salt particles below 500 m compete with heterogeneous loss in clouds droplets. Increasing one heterogeneous process merely causes the remaining heterogeneous process to oxidize less SO_2. Thus deviation from the baseline scenario is much less effective.

A fraction of the sea salt particles mass lies in the submicronic part of the aerosol distribution. *Quinn et al.* [1998] estimate that the majority of the concentration of sea salt aerosol mass occured in the supermicron size range (90 ± 2%). Thus, about 10% of nss sulfate produced from oxidation of SO_2 by O_3 in the sea salt contributes to the total mass of submicron nss sulfate in the model. The remaining 90% are assumed to rapidly redeposited at the ocean surface with the supermicronic sea salt.

2.2.6. Scavenging of aerosol nss sulfate and MS. In this section, we describe the cloud microphysics and scavenging parameterizations. The representation of cloud microphysics is a bulk-water parameterization which includes mixing ratios of water vapor (r_v in kg/kg), cloud water (r_c in kg/kg) and rain water (r_v in kg/kg). A parallel parameterization is adopted to represent the scavenging interactions between aerosols and hydrometeors including collection of particles due to condensation nucleation and resuspension because of evaporation. Note that the rain water reservoir is also implemented in the model with the corresponding interactions with aerosols (e.g., accretion, autoconversion, inertial capture). Precipitation scavenging, although the primary mechanism for removing small aerosol particles will not be described here as no rain was neither observed nor simulated during Lagrangian B experiment.

Particles ingested into a cloud can be incorporated into a cloud hydrometeor by condensation. Once they are collected, we assume they are well-mixed and move with the hydrometeors [*Molenkamp and Bradley*, 1992]. The collected particles are eventually resuspended when the cloud evaporates.

The evaporation terms (source of dry nss sulfate and sink of nss sulfate in cloud water) are proportional to the water transfer rate (P_{EVAP}, in kg kg^{-1} s^{-1}) between water vapor

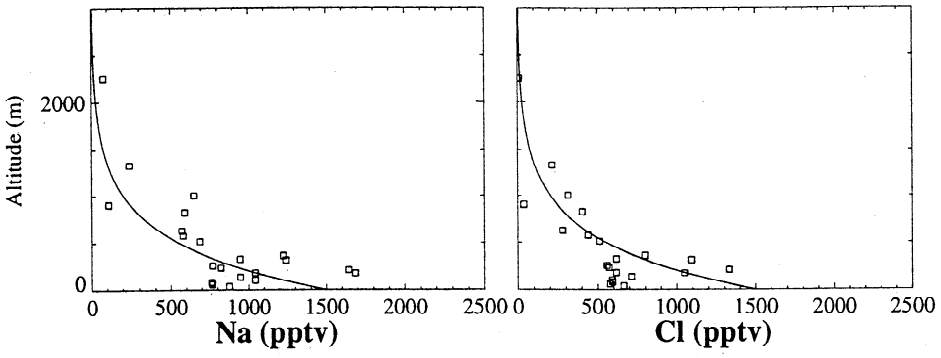

Figure 4. Vertical profiles of sodium Na^+ and chloride Cl^- mixing ratios (in pptv) during the Lagrangian B. The solid line is an exponential function fitted over the data.

and cloud water because of the well-mixed assumption and are given by

$$Q^{\text{trans}}_{\text{SO}_4^= a} = -Q^{\text{trans}}_{\text{SO}_4^= c} = \frac{\text{SO}_4^= c}{r_c} P_{\text{EVAP}}$$

where $Q^{\text{trans}}_{\text{SO}_4^= c}$ and $Q^{\text{trans}}_{\text{SO}_4^= a}$ represent the transfer rates, in pptv s^{-1}, between nss sulfate in cloud water and dry nss sulfate reservoirs.

The condensation nucleation scavenging terms are represented by

$$Q^{\text{trans}}_{\text{SO}_4^= a} = -Q^{\text{trans}}_{\text{SO}_4^= c} = -\epsilon \frac{\text{SO}_4^= a}{\Delta t}$$

where $\epsilon = 0.55$. This value has been fixed so that 94% of the aerosols are incorporated in the hydrometeors within the 100 s following the cloud formation [*Jensen and Charlson*, 1984; *Flossman et al.*, 1985; *Rutledge et al.*, 1986]. This term is activated only at grid point where the condensation rate for cloud water is positive.

3. Results and Discussion

3.1. Dynamics

Figure 5 gives the observed versus simulated potential temperature, wind speed, and vapor mixing ratio for each individual observed points. Model values are shown at the closest time and height of observations. Also shown in this plot are the least squares correlation coefficient (r^2) between model and observations, the slope (s) of the linear fit obtained by the multilinear regression method [*Bevington*, 1969], and the median ratio (R) of simulated-to-observed concentrations. Both $s$and Roffer different measures of model bias. The model captures 96% of the observed variance of potential temperature without bias (R=0.99, and s=0.93). The model is also able to reproduce properly the observed vapor mixing ratio (r^2=0.85, R=1.03 and s=0.95). The increase of wind speed along the Lagrangian B trajectory is captured by the model (r^2=0.85, R=1.18 and s=0.96) although the model tends to slightly overestimate the wind speed during flight 26.

3.2. DMS

3.2.1. Comparison with the C-130 observations. Figure 6 compares simulated and observed DMS mixing ratios for each individual observed points. We find that the model captures 82% of the variance of the observed DMS mixing ratios assuming OH is the only oxidant and a DMS flux parameterization based on *Liss and Merlivat* [1986]. The median simulated-to-observed concentration ratio is 0.92, and the linear regression slope is 0.77, showing that the model tends to slightly underestimate the DMS mixing ratios.

Figure 7 reveals the vertical structure of DMS mixing ratios for each sounding during Lagrangian B. Also shown on this plot are the profiles obtained when using a DMS flux based on *Wanninkhof* [1992] and an additional sink for DMS comparable to the oxidation by OH [*Chin et al.*, 1996]. It is worth emphasizing that no DMS, SO_2, MS, or nss sulfate measurements were made during the aircraft soundings.

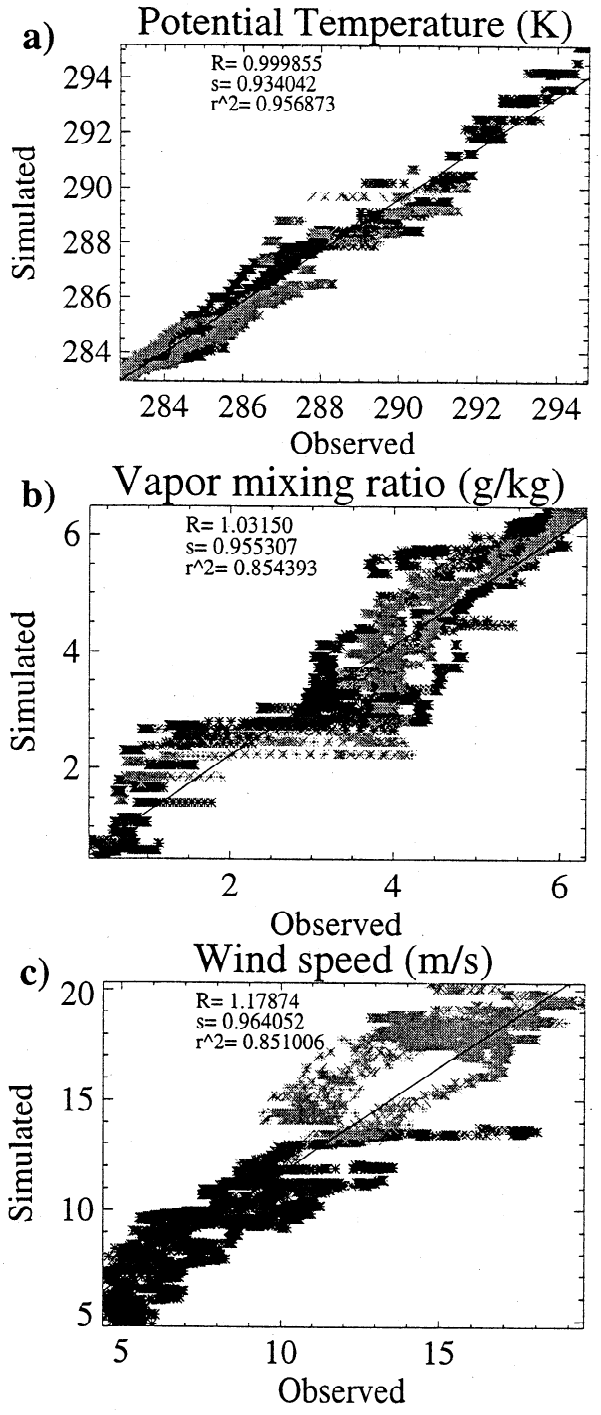

Figure 5. Simulated versus observed (a) potential temperature in K, (b) vapor mixing ratio in g/kg, and (c) wind speed in m/s during Lagrangian B. Also shown are the linear regression line, the least squares correlation coefficient (r^2), the slope of the regression line (s) and the median ratio of simulated to observed concentrations (R). Stars corresponding to flight 24 are in black, flight 25 in dark gray, and flight 26 in light gray.

The data presented here were measured when the aircraft flew along constant altitude circles at various levels. Observations that were taken closer than 1.5 hours to the indicated aircraft soundings are marked by a diamond, and the remaining data

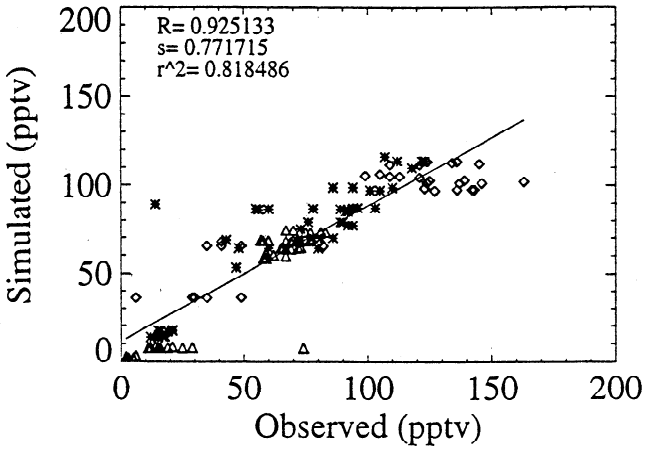

Figure 6. Simulated versus observed DMS mixing ratios during Lagrangian B for flight 24 (stars), flight 25 (triangles), and flight 26 (diamonds). Also shown are the linear regression line, the least squares correlation coefficient (r^2), the slope of the regression line (s), and the median ratio of simulated to observed mixing ratios (R). The number of observed points is 128.

are marked by a cross. DMS vertical profiles reveal a two-layer structure in the marine boundary layer . High mixing ratios characterized the lower well mixed layer between 0 and 500 m during flights 24 and 25. Lower values prevail in the upper layer. Simulated and observed DMS in the free troposphere show near-zero mixing ratios. During flight 26, concentrations near the surface increase due to maintained high values of DMS flux (see Figure 3). Higher values are simulated and observed at higher altitudes (30 pptv at 1400 m) due to the redistribution of DMS throughout the vertical column by cloud mixing at the end of the experiment. In the case where the parameterization of *Wanninkhof* [1992] and an additional reaction for DMS are used, the model captures 83 % of the observed variance of DMS mixing ratios. The median simulated-to-observed concentration ratio is 1.14, and the linear regression slope is 1.18 showing that, in this case, the model tends to slightly overestimate the DMS mixing ratios.

We now turn to the time serie of averaged DMS mixing ratios in the lower well mixed layer between 0 and 500 m. As shown in Figure 8, the model successfully reproduces the diurnal variation of DMS, with a more pronounced cycle when using DMS flux calculated using *Wanninkhof* [1992] and an additional reaction. The difference between both simulations is highest (about 50 %) during flight 26 due to the combined effect of strong wind speed near the surface and low oxidation of DMS under cloud topped layer. The mean residence time for DMS is 22 hours in the reference case but decreases to 11 hours using the *Wanninkhof* [1992] DMS flux and additional oxidation reaction.

3.2.2. Discussion. The model is able to reproduce the observed DMS mixing ratios levels, the vertical distribution, and the amplitude of DMS diurnal variation. The sensitivity study on flux parameterizations, however, identify a best fit wind speed transfer velocity relationship due to the uncer-

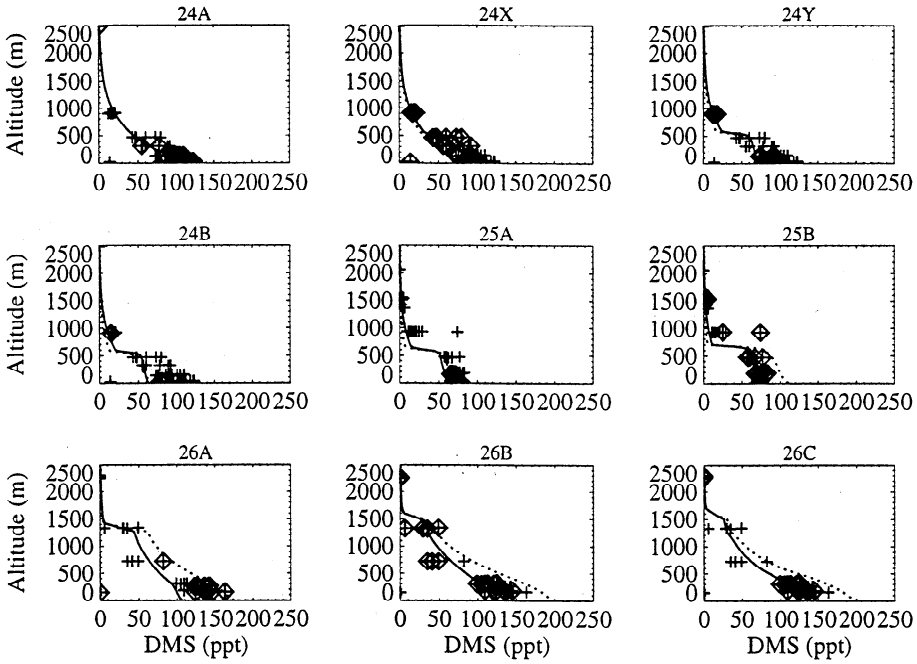

Figure 7. Dimethylsulfide (DMS) mixing ratios in pptv for the nine aircraft soundings during Lagrangian B. No measurements of DMS were performed during the soundings. Measurements made during horizontal circles that are closer than 1.5 hours to aircraft sounding are presented by diamonds, and other data from the same flight are indicated by crosses. The simulation using flux calculated from *Liss and Merlivat* [1986] wind speed transfer velocity relationship is represented by the solid line, and simulation using the flux calculated from the *Wanninkhof* [1992] wind speed transfer velocity relationship is represented by the dotted line. The detection limit for DMS measurements is 1 pptv, and precision is 1 pptv.

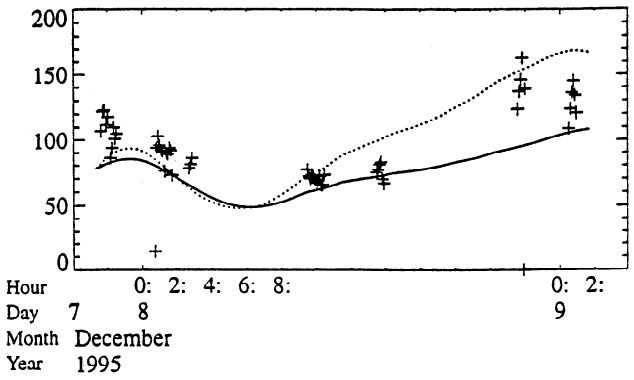

Figure 8. Time series of DMS mixing ratios in pptv averaged between the surface and 500 m (a) assuming a flux calculated using *Liss and Merlivat* [1986] and OH as the only oxidant (solid line) and (b) assuming a flux calculated using *Wanninkhof* [1992] and an additional reaction for DMS (dotted line).

tainties on DMS oxidation rates and regional seawater DMS concentrations [*Mari et al.*, 1998]. This points to a major gap in current understanding of the processes that control DMS concentrations. In the baseline scenario, we assume that DMS chemical consumption is only due to oxidation by the OH radical and we use a branching ratio to predict the oxidation products of DMS. The use of simplified schemes has been adopted in global atmospheric chemistry models [*Benkovitz et al.*, 1994; *Pham et al.*, 1995; *Chin et al.*, 1996; *Feichter et al.*, 1996]. *Capaldo and Pandis* [1997] point out that the variations among the gas phase mecanisms are small with the parameterized mecanisms performing as accurately as the comprehensive ones. Several studies have shown that oxidation of DMS by OH is adequate to simulate DMS levels [*Bandy et al.*, 1996; *Mari et al.*, 1998; *Suhre et al.*, 1998]. However, several studies have needed a factor of 2 increase of DMS oxidation rate to reproduce the DMS diurnal cycle [*Suhre et al.*, 1995; *Yvon et al.*, 1996; *Chin et al.*, 1996, 1998]. The need for higher DMS oxidation rate can be attributed to unaccounted DMS oxidants or oxidation pathways, such as reaction with halogen species (Cl, Br, BrO) [*Pszenny et al.*, 1993; *Toumi*, 1994]. Halogenated radicals are expected to be more reactive with DMS than OH radical and could explain the rapid decline of DMS concentrations at dawn even though no field study has convincingly demonstrated this point.

In addition to these uncertainties in DMS oxidation rates, there are currently no directly measured DMS fluxes. It is typically assumed that the DMS emission rate is dependent on seawater DMS concentration and wind speed. However, the details of how the wind speed, diffusivity, thermal stability, sea state, organic films [*Frew*, 1997], sea surface microlayers, chemical reactions in surface seawater, and other factors influence the transfer velocity and the sea-air exchange of DMS are not clearly understood [*Erickson*, 1993]. These considerations, however, do not necessarily increase the uncertainty ranges (more than a factor of 2 currently) of the calculated transfer velocity at a given wind speed. Rather, they invalidate the assumption that there is a single, "correct" parameterization of transfer velocity based on wind speed alone [*Chin et al.*, 1998]. Thus the comparison of DMS oxidation products such as SO_2 and nss sulfate is needed in order to provide a more constrained evaluation of model processes such as emission flux and oxidation rate. We discuss the case of SO_2 in the following section.

3.3. SO_2

3.3.1. Comparison with the C-130 observations. Figure 9 compares simulated and observed SO_2 mixing ratios for each individual observed points. The model captures 75% of the observed variance. Median simulated-to-observed concentration ratio is 0.99, and the slope of the regression line is 1.11. Thus the model reproduces SO_2 mixing ratios without bias.

Vertical profiles for SO_2 are shown in Figure 10. Again, a two-layer structure is simulated in agreement with the observations during flight 24. During the first flight, a mixed rich lower layer agrees generally well with the observations, increasing from 40 pptv during sounding 24A to 60 pptv during sounding 24B near the surface. During flight 25, elevated mixing ratios were measured (20 pptv at 1500 m) that are not reproduced by the model. These high mixing ratios during the nocturnal flight are likely to be due to differential advection and/or sampling uncertainties on the aircraft circles. It is worth noting that the central assumption for the model and the experiment is that horizontal advection can be ignored. However, the significant shear [*Russell et al.*, 1998; *Suhre et al.*, 1998] indicates that the difference in the advection rates of the lower (below 1000 m) and upper layer could be significant, particularly during the end of flight 25 and during flight 26. During flight 26, mixing ratios of SO_2 decrease in

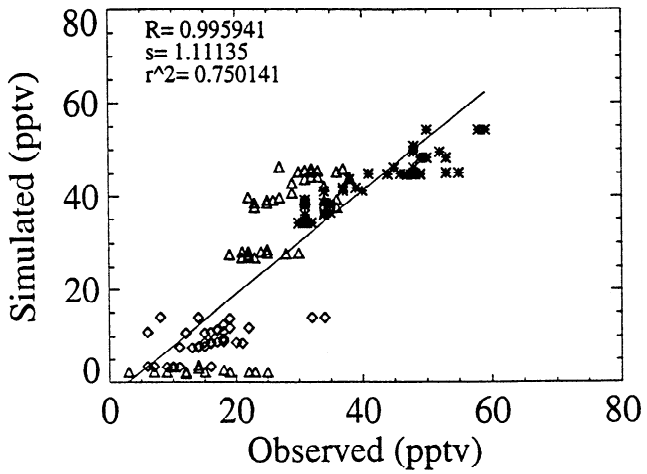

Figure 9. Simulated versus observed SO_2 mixing ratios during Lagrangian B for flight 24 (stars), flight 25 (triangles), and flight 26 (diamonds). Also shown are the linear regression line, the least squares correlation coefficient (r^2), the slope of the regression line (s), and the median ratio of simulated to observed concentrations (R). The number of observed points is 144.

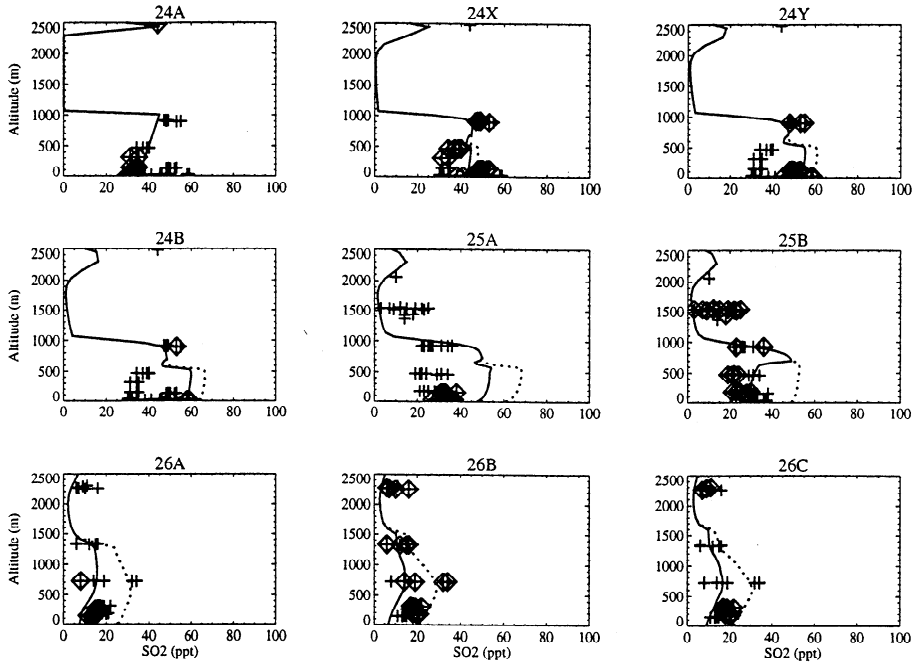

Figure 10. Sulfur dioxide (SO_2) mixing ratios in pptv for the nine aircraft soundings during Lagrangian B. No measurements of SO_2 were performed during the soundings. Measurements made during horizontal circles that are closer than 1.5 hours to aircraft sounding are presented by diamonds, and other data from the same flight are indicated by crosses. The simulation without loss of SO_2 in sea salt is represented by the dotted line, and the simulation in the reference case with loss in sea salt is represented by the solid line. The detection limit for SO_2 measurements is 1 pptv, and precision is 1 pptv.

both measurements and model during flight 26 due to combined effect of heterogeneous loss in cloud droplets and sea-salt particles. Also shown in Figure 10 are the simulated SO_2 mixing ratios when the loss in sea-salt particles is removed. Without heterogeneous loss in sea-salt, SO_2 predictions are 5% higher during flight 24 (under weak wind speed conditions) to 100% higher during flight 26 (under strong wind speed conditions). Neglecting heterogeneous loss in sea-salt particles deteriorates the simulation, and the model captures only half of the observed variance ($r^2 = 0.5$).

The diurnal cycle of SO_2 is averaged in Figure 11 in the lower layer below 500 m. Also shown in this figure are the diurnal cycles obtained (1) without heterogeneous loss in sea-salt and (2) assuming that the additional reaction, needed to recover the levels of DMS when a DMS flux of *Wanninkhof* [1992] is used, produces SO_2 with a 100% yield [*Chin et al.*, 1996]. The effect of removing heterogeneous loss in sea-salt particles is particularly sensitive during flights 25 and 26 when the oxidation rate of SO_2 increases over 10%/h (see Figure 3) due to the increase of wind speed near the surface. It is noted that the assumption of an additional source of SO_2 from oxidation of DMS leads to an overestimate of the SO_2 concentrations during flights 24 and 25. This difference is reduced during flight 26 due to the relatively high SO_2 heterogeneous oxidation in cloud droplets and sea-salt particles in the lower layer.

3.3.2. Discussion. DMS to SO_2 conversion efficiency is calculated as the ratio of the chemical source terms of SO_2 from DMS to the chemical sink term of DMS. In the case where a branching ratio of 0.6 is assumed for the addition pathway, the DMS to SO_2 conversion efficiency is 60, 71, and 74% for flights 24, 25, and 26 respectively. *De Bruyn et al.* [1998] found that the DMS to SO_2 conversion efficiency during the ACE 1 study ranged between 30 and 50%. These values are well below that actually used in this model to simulate SO_2 mixing ratios. The DMS to SO_2 ratio calculated from the aircraft measurements vary from 0 to 10 with

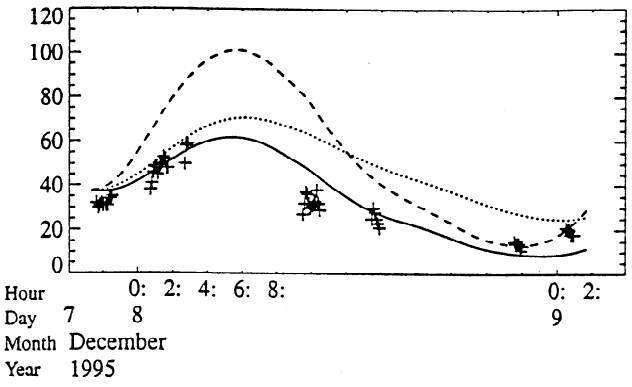

Figure 11. Time series of SO_2 mixing ratios in pptv averaged between the surface and 500 m (a) in the reference case (solid line) (b) assuming no loss of SO_2 in sea-salt particles (dotted line), and (c) assuming a flux calculated using *Wanninkhof* [1992] and an additional reaction of DMS which gives SO_2 with a 100% yield (dashed line).

a mean value of 3.6 ± 2.6 and a median value of 1.9. These values are 4 times lower than those obtained by *De Bruyn et al.* [1998]. This low value of DMS to SO_2 ratio deduced from the aircraft measurements explains the higher value of the DMS to SO_2 conversion efficiency needed in this study compared to the one estimated from the ship measurements.

During the Lagrangian B experiment, SO_2 sink in sea salt, averaged over the well mixed lower layer, is 6400 mol cm^{-3} s^{-1} during flight 24, 16000 mol cm^{-3} s^{-1} during flight 25, and 4700 mol cm^{-3} s^{-1} during flight 26. These sinks are comparable to the values of 7000 mol cm^{-3} s^{-1} calculated by *Sievering et al.*, [this issue] from measurements of nss sulfate in large aerosols at Cape Grim during ACE 1. These values are 1 to 5 times higher than those calculated by *De Bruyn et al.* [1998] from the measurements of nss sulfate in large aerosols on board R/V *Discoverer* but comparable to the values these authors used for their box model calculation to fit the data. From this comparison, it is worth noting that the still existing uncertainties on the removal rates of SO_2 in sea salt prevent to better quantify the processes controlling the sulfur budget.

Loss of SO_2 in sea-salt particles is a major process for the SO_2 budget in the ACE 1 region. Several authors have suggested that uptake of SO_2 by sea-salt aerosols may provide a large sink in the marine boundary layer [*Sievering et al.*, 1991, 1992, 1995; *Suhre et al.*, 1995; *Chameides and Stelson*, 1992; *O'Dowd et al.*, 1997]. It is worth emphasizing that our parameterization of sea salt particles is simplified and does not take into account either chemistry or pH evolution within sea salt aerosols. Scavenging of SO_2 and the subsequent oxidation of dissolved SO_2 by ozone under alkaline conditions has been reported to be the principal source of nss sulfate in the sea-salt aerosol. Production via this pathway is limited by diffusion of SO_2 into the aerosol and available alkalinity. Alkalinity (i.e., the measure of the buffering capacity of a solution) is widely assumed to derive solely from the parent seawater and to be titrated rapidly (less than an hour) by H_2SO_4 [*Chameides and Stelson*, 1992]. This titration lowers solution pH and depresses SO_2 solubility, and the ozone oxidation pathway becomes negligible. However, several authors have suggested that another oxidation pathway such as reaction with HOCl or HOBr may be important [*Sander and Crutzen*, 1996; *Vogt et al.*, 1996, *Keene and Savoie*, 1998]. Although slower than reaction with ozone, these reactions are not limited by available alkalinity and proceed at significant rates over the relatively long lifetime of the sea salt aerosol (1 to 2 days). Pathways involving photolysis of dissolved organic compounds may also contribute [*Keene et al.*, 1998]. The buffering capacity available to maintain this rapid SO_2 depletion pathway may also be enhanced by carbonate/bicarbonate from biogenic material in the surface layer [*Sievering et al.*, this issue].

Figure 12 shows the budget terms for SO_2 averaged on each flight: turbulent mixing which is representative of dry deposition sink, homogeneous oxidation of DMS by OH, heterogeneous oxidation of SO_2 in cloud droplets, and in sea salt particles and homogeneous reaction of SO_2 with OH. It is worth noting that loss of SO_2 to sea-salt is competitive with loss by dry deposition during flight 24 and higher during the last two flights. Relative contributions of these terms averaged over the entire column are given in Table 3. During all flights, except the first one, heterogeneous oxidation in sea-

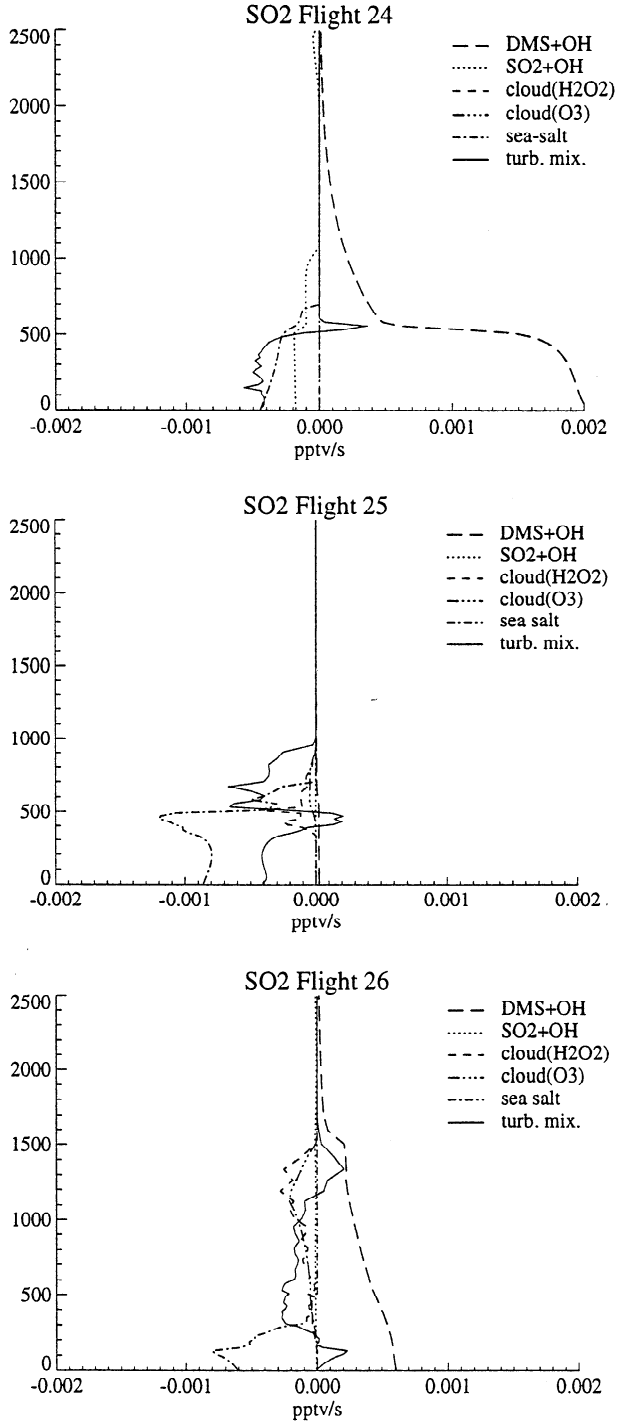

Figure 12. Vertical profiles of source and sink terms of SO_2 in pptv/s. Profiles are averaged over each flight period. Sources and sinks included homogeneous oxidation of DMS by OH (long-dashed line), homogeneous oxidation of SO_2 by OH (dotted line), heterogeneous oxidation of SO_2 to nss sulfate in clouds by H_2O_2 (dashed line), and O_3 (dash-triple-dotted line), heterogeneous oxidation of SO_2 to nss sulfate by O_3 in sea salt (dash-dotted line), and turbulent mixing (solid line)

Table 3. SO_2 Budget

	Relative Contribution, %		
	Flight 24	Flight 25	Flight 26
OH oxidation	24	0	2
Sea-salt aerosols	37	63	41
Turbulent mixing (dry deposition)	39	29	22
Incloud oxidation (H2O2)	0	6	16
Incloud oxidation (O3)	0	2	19
Total incloud oxidation	0	8	35

salt particle is the largest sink of SO_2 . Turbulent mixing (dry deposition) contributes to 39, 29, and 22%, respectively, to the total budget of SO_2. The relative contribution of in-cloud oxidation to the SO_2 budget is negligible during flights 24 and 25 (0 and 8%, respectively). During flight 25, as clouds form in the lower layer, SO_2 is oxidized mainly by H_2O_2. During flight 26, heterogeneous oxidation in cloud droplets under about 1200 m is mainly due to ozone whereas H_2O_2, consumed at lower altitude, is the main oxidant above 1200 m. The relative contribution of in-cloud oxidation during flight 26 is comparable to the loss in sea-salt particles (35%). The mean SO_2 lifetime is 11 hours during Lagrangian B experiment, driven mainly by dry deposition and loss in sea-salt particles.

3.4. MS

3.4.1. Comparison with the C-130 observations. Figure 13 compares simulated and observed MS mixing ratios for each individual observed points. The model captures 62.5% of the observed variance. Median simulated-to-observed concentration ratio is 1.25, and the slope of the regression line is 1.87. Thus the model tends to overestimate the observed concentrations during Lagrangian B in the reference simulation. Our ability to interpret model results for MS is evidently hampered by the small number of observed points (n=23).

Figure 14 illustrates the evolution of MS vertical profiles during Lagrangian B in the reference scenario and for a 0.8 branching ratio. As for DMS, a rich lower layer is observed and modeled below 500 m during flights 24 and 25. In the reference case, however, during flight 25, MS mixing ratios are overestimated by a factor of 2 below 500 m. During flight 26, cloud mixing pumps MS to higher altitudes where precursors are also present. Again, the model overestimates MS mixing ratios near the surface. Simulation of MS can be improved by using a branching ratio (α) for the addition pathway of 0.8 (r^2= 0.59, s= 1.13, R= 0.96). Simulated SO_2 mixing ratios are still comparable with the measurements and only 10% higher than in the reference case.

Figure 15 shows the temporal evolution of MS mixing ratios in the lower well mixed layer, below 500 m. It appears that MS mixing ratios exhibit a diurnal cycle in both model and observations. MS increases throughout the day, then decreases at night. Again, using a branching ratio of 0.8 improves the simulation of MS.

3.4.2. Discussion. MS mixing ratios are very sensitive to the choice of the branching ratio. The DMS to MS conversion efficiency in the model is respectively 22, 22, and 24%, respectively, during flights 24, 25, and 26 in the reference case. Best results are obtained when the DMS to MS conversion efficiency is lower (around 10%). These values are comparable with the one obtained by *Benkovitz et al.* [1994] in the northern hemisphere ocean of almost 13%. In conclusion, the simple DMS oxidation scheme used in this study requires high branching ratio for the addition pathway to recover both SO_2 and MS levels.

3.5. Nss sulfate

3.5.1. Comparison with the C-130 observations. Figure 16 compares simulated and observed nss sulfate mixing ratios for each individual observed points. The model captures only 32% of the observed variance. Median simulated-to-observed concentration ratio is 1.03, and the slope of the regression line is 0.7. Thus the model predicts the nss sulfate observed mixing ratios with little bias but simulates only one third of the observed variance. Our ability to interpret

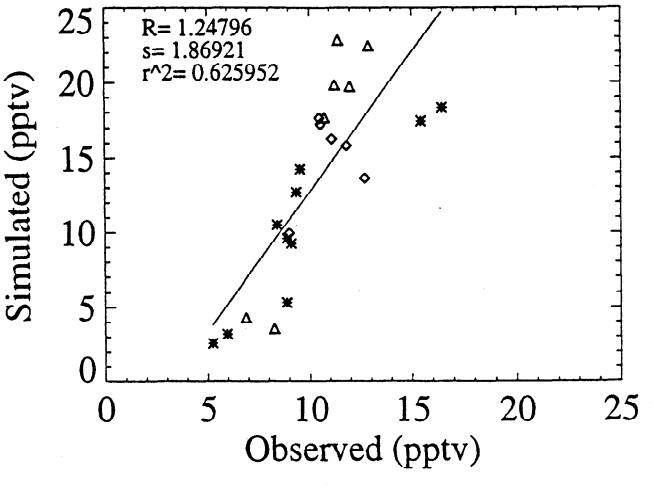

Figure 13. Simulated versus observed MS mixing ratios during Lagrangian B for flight 24 (stars), flight 25 (triangles), and flight 26 (diamonds). Also shown are the linear regression line, the least squares correlation coefficient (r^2), the slope of the regression line (s) and the median ratio of simulated to observed concentrations (R). The number of observed points is 23.

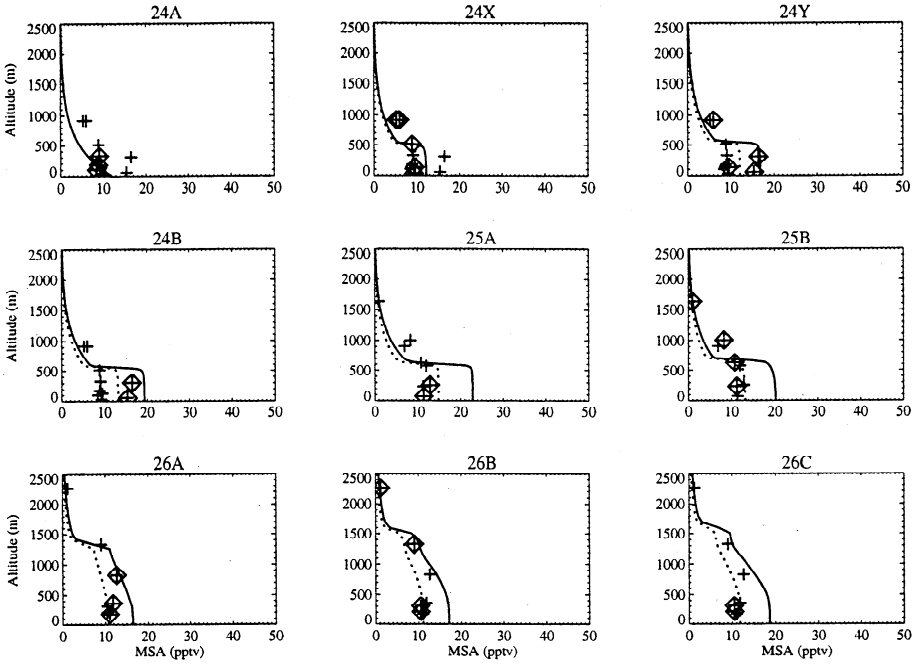

Figure 14. Methanesulfonate (MS) mixing ratios in pptv for the nine aircraft soundings during Lagrangian B. No measurements of MS were performed during the soundings. Measurements made during horizontal circles that are closer than 1.5 hours to aircraft sounding are presented by diamonds, and other data from the same flight are indicated by crosses. The simulation with a branching ratio for the addition oxidation pathway of 0.8 is represented by the dotted line, and the simulation in the reference case (with branching ratio 0.6) is represented by the solid line.

model results for nss sulfate is evidently hampered by the small number of observed points (n=24).

We now turn to the vertical profiles of nss sulfate mixing ratios (Figure 17). The major discrepancies are obtained above 500 m during flights 25 and 26 where the model tends to underestimate the mixing ratios. It is worth noting that high nss sulfate concentrations were measured above 3000 m (200 pptv at 4500 m) [*Huebert et al.*, 1998], suggesting that nss sulfate concentrations increase with altitude above 1 km. This increase of nss sulfate concentrations with altitude is not taking into account in the initial profile. We suggest that this can explain most of the discrepancy obtained above 1000 m during flights 25 and 26 where combination of a higher turbulent mixing and subsidence at the top of the column could have entrained higher nss sulfate concentrations in the boundary layer.

Nss sulfate mixing ratios show a weak diurnal cycle in the lower well mixed layer (Figure 18). The observed submicron nss sulfate mixing ratio increased in the daytime and sta-

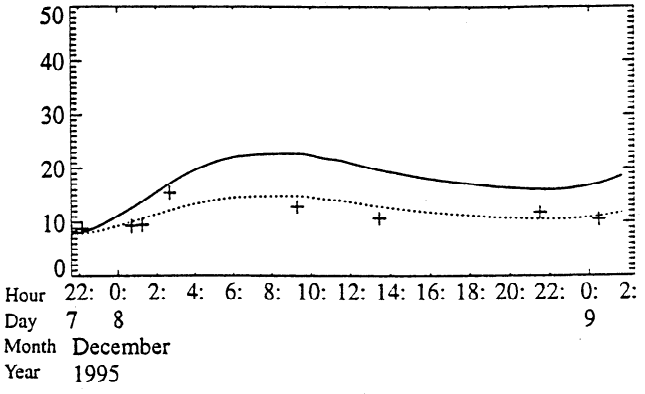

Figure 15. Time series of MS mixing ratios in pptv averaged between the surface and 500 m in the reference case (solid line), and assuming a branching ratio of 0.8 (dashed line).

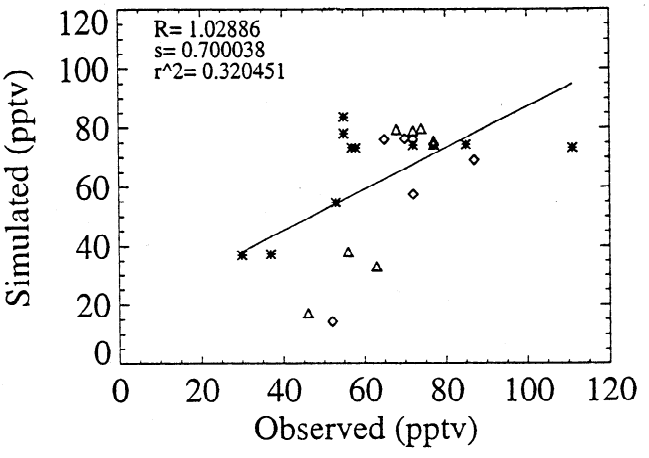

Figure 16. Simulated versus observed nss sulfate mixing ratios during Lagrangian B for flight 24 (stars), flight 25 (triangles), and flight 26 (diamonds). Also shown are the linear regression line, the least squares correlation coefficient (r^2), the slope of the regression line (s), and the median ratio of simulated to observed concentrations (R). The number of observed points is 24.

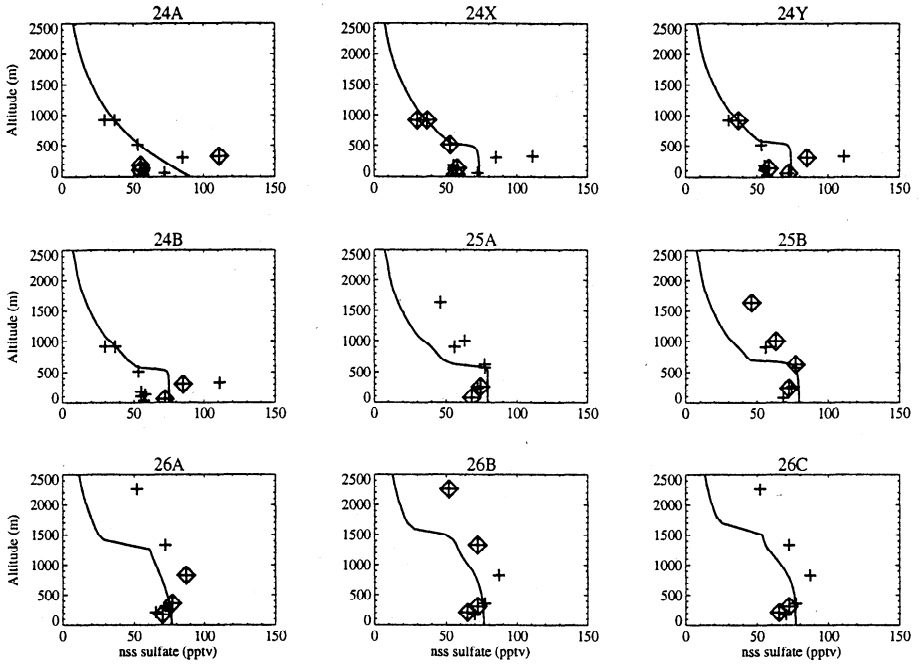

Figure 17. Nss sulfate mixing ratio in pptv for the nine aircraft soundings during Lagrangian B. No measurements of nss sulfate were performed during the soundings. Measurements made during horizontal circles that are closer than 1.5 hours to aircraft sounding are presented by diamonds, and other data from the same flight are indicated by crosses.

bilized at night. The model reproduces this evolution very well. The doubling in SO_2 mixing ratios, especially during flight 24, by using the *Wanninkhof* [1992] wind speed transfer velocity relationship and an additional reaction does not change the simulated nss sulfate mixing ratios by more than 10 % during the 30 hours duration of the Lagrangian B.

3.5.2. Discussion. The observed and simulated diurnal variation of nss sulfate mixing ratios would seem to confirm that some nss sulfate is produced photochemically [*Huebert et al.*, 1998] at least under non cloudy low wind speed conditions encountered during flight 24. Vertical profiles averaged for each flight of nss sulfate budget are shown in Figure 19. Table 4 gives the averaged relative contribution of each source term over the whole column for each flight. During flights 25 and 26, nss sulfate is produced by nonphotochemical mechanisms such as oxidation in the cloud droplets or in sea salt. During flight 25, oxidation in cloud droplets begins around 500 m and contributes to 48% to the source of nss sulfate. As wind speed increases, the production of sea salt near the surface is enhanced. Oxidation of SO_2 in submicron sea salt contributes 50% to the source of nss sulfate. During flight 26, in-cloud oxidation of SO_2 is the main source of nss sulfate (69%) with oxidation occuring around 1000 m. Below this altitude, SO_2 has been consumed in the lower layer of clouds and in the sea-salt particles, thus limiting the effect of in-cloud oxidation.

The observed mean MS to nss sulfate molar ratio in the submicron particles is 0.15 ± 0.04. The modeled ratio is 0.23 ± 0.05 which compares well with the observations, although slightly higher. This ratio is also close to the ratio calculated on board the R/V *Discoverer* of 0.22 ± 0.16 [*Quinn et al.*, 1998].

4. Conclusions

A 1-D Lagrangian model has been used to simulate vertical profiles and temporal evolution of DMS, SO_2, aerosol MS, and nss sulfate that were measured during the Lagrangian B experiment. The model was able to reproduce correctly the vertical structure of the column and absolute values of potential temperature, water vapor, wind speeds and cloud water when forced only with geostrophic wind and synoptic-scale

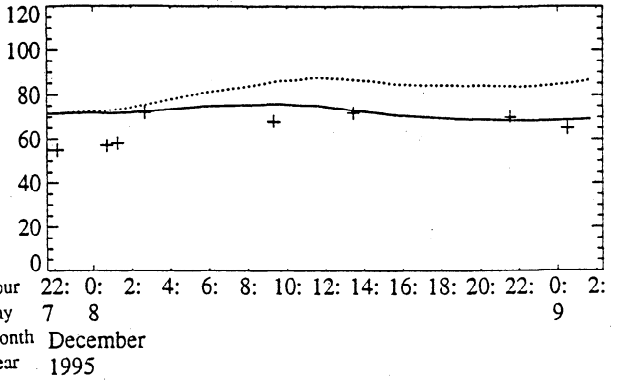

Figure 18. Time series of nss sulfate mixing ratios in pptv averaged between the surface and 500 m (a) in the reference case (solid line), (b) assuming flux from *Wanninkhof* [1992] and an additional reaction of DMS producing SO_2 with a 100% yield (dotted line).

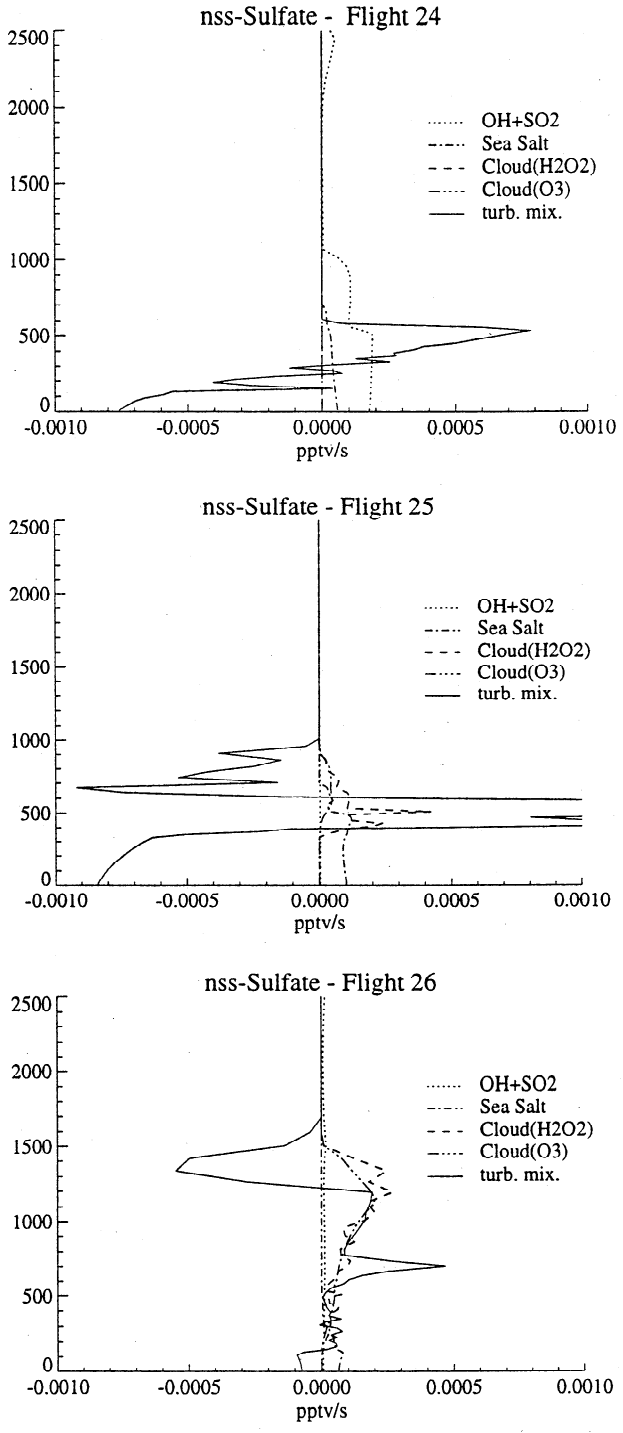

Figure 19. Vertical profiles of source and sink terms of nss sulfate in pptv/s. Profiles are averaged over each flight period. Sources and sinks included homogeneous oxidation of SO_2 by OH (dotted line), heterogeneous oxidation of SO_2 to nss sulfate in clouds by H_2O_2 (dashed line), and O_3 (dash-triple-dotted line), heterogeneous oxidation of SO_2 to nss sulfate by O_3 in sea salt (dash-dotted line), and turbulent mixing (solid line)

subsidence adapted from ECMWF analysis and SST measured on board the R/V *Discoverer*.

The model captures 82% of the variance of observed DMS assuming OH is the only oxidant and a DMS flux calculated using the *Liss and Merlivat* [1986] wind speed transfer velocity relationship and seawater DMS measured aboard R/V *Discoverer*. Similar agreement was obtained (r^2= 83%) when using the *Wanninkhof* [1992] wind speed transfer velocity relationship and an additional reaction for DMS oxidation. Thus no conclusion can be drawn concerning the most appropriate wind speed transfer velocity relationship due to the uncertainties in DMS oxidation rates. Comparison of DMS products is thus needed to provide a better constraint of model results.

SO_2 mixing ratios were correctly represented in the model (r^2= 75%) using a simple oxidation scheme with a DMS to SO_2 conversion efficiency of about 70%. Removing heterogeneous loss of SO_2 in sea salt deteriorates the simulation (r^2= 50%). Oxidation of SO_2 in sea-salt particle appeared to be a dominant process and controlled SO_2 lifetime during the Lagrangian B in the well mixed lower layer. Under cloudy conditions, heterogeneous loss in cloud droplets and in sea-salt particles were competitive (relative rates are 35 and 41%, respectively, during flight 26). Heterogeneous loss of SO_2 in sea-salt particles was found to be comparable or greater than loss by dry deposition, especially under high wind speed conditions when sea-salt production was enhanced.

MS mixing ratios were correctly reproduced by the model (r^2= 62.5%) when a branching ratio for additional oxidation pathway of 0.6 was used. Simulation of MS was improved if a higher branching ratio was applied, corresponding to a DMS to MS conversion efficiency of 10%.

The model reproduced nss sulfate mixing ratios with little bias (median simulated-to-observed concentration ratio equal to 1.03 and slope of the regression line 0.7) but captured only one third of the observed variance of nss sulfate. High mixing ratios were measured at 4500 m, suggesting an increase of nss sulfate with altitude above the inversion level that was not taking into account in the model. This observed increase of nss sulfate with altitude suggests that horizontal advection is a dominate process in this region that cannot be captured by such Lagrangian model. Nss sulfate was found to be produced photochemically under non cloudy, low wind speed conditions encountered during flight 24. During the last two flights, nss sulfate was produced by oxidation in cloud droplets (48% during flight 25 and 69% during flight 26) and sea-salt particles (50% during flight 25 and 22% during flight 26). Overall, the detailed measurements made in Lagrangian framework, combined with a 1-D model provided sufficient constraints to enhance our understanding of the processes con-

Table 4. The nss sulfate Budget

	Relative Contribution, %		
	Flight 24	Flight 25	Flight 26
OH oxidation	83	2	9
Sea-salt aerosols	17	50	22
Incloud oxidation (H2O2)	0	39	35
Incloud oxidation (O3)	0	9	34
Total incloud oxidation	0	48	69

trolling the sulfur budget in the ACE 1 region. Comparisons with the measurements also emphasized the still existing uncertainties that prevent better quantification of the sulfur budget during the ACE 1 experiment including the DMS flux at the sea surface, the DMS oxidation rates and products, and the removal of SO_2 by sea salt aerosol.

Acknowledgments. This research is a contribution to the International Global Atmospheric Chemistry (IGAC) Core project of the International Geosphere-Biosphere Programme (IGBP) and is part of the IGAC Aerosol Characterization Experiments (ACE). We gratefully acknowledge rapid access to all ACE 1 data via the UCAR/JOSS office. Of particular use for this study were data on wind speed, temperature, and humidity from the NCAR/C130, and GMS and NOAA satellite images. Analyzed synoptic scale meteorological data originate from the ECMWF archive MARS. Computing resources were provided by CNRS/IDRIS and Meteo France. Some financial support was provided by CNRS program PATOM.

References

Atkinson, R., D.L. Baulch, R.A. Cox, R.F. Hampson, J.A. Kerr, and J. Troe, Evaluated kinetic and photochemical data for atmospheric chemistry: Supplement IV, *Atmos. Environ., Part A, 26,* 1187–1230, 1992.

Ayers, G.P., R.W. Gillett, J.P. Ivey, B. Schäfer, and A. Gabric, Short-term variability in marine atmospheric dimethylsulfide concentration, *Geophys. Res. Lett., 22,* 2513–2516, 1995.

Bandy, A.R., D.C. Thornton, B.W. Blomquist, S. Chen, T.P. Wade, J.C. Ianni, G.M. Mitchell, and W. Nadler, Chemistry of dimethyl sulfide in the equatorial Pacific atmosphere, *Geophys. Res. Lett., 23,* 741–744, 1996.

Bates, T.S., B.J. Huebert, J.L. Gras, B. Griffiths and P. Durkee, The International Global Atmopsheric Chemistry (IGAC) Project's First Aerosol Characterization Experiment (ACE 1): Overview, *J. Geophys. Res., 103,* 16,297–16,318, 1998a.

Bates, T.S., V.N. Kapustin, P.K. Quinn, D.S. Covert, D.J. Coffman, C. Mari, P.A. Durkee, W.J. DeBruyn, and E. Satzman, Processes controlling the distribution of aerosol particles in the marine boundary layer during ACE 1, *J. Geophys. Res., 103,* 16,369–16,383, 1998b.

Benkovitz, C.M., C.M. Berkovitz, R.C. Easter, S. Nemesure, R. Wagener, and S. Schwartz, Sulfates over the North Atlantic and adjacent continental regions: Evaluation for October and November 1986 using a three-dimensional model driven by observation-derived meteorology, *J. Geophys. Res., 99,* 20,725–20,756, 1994.

Berresheim, H., M.O. Andreae, G.P. Ayers, R.W. Gillett, J.T. Merrill, V.J. Davis, and W.L. Chameides, Airborne measurements of dimethylsulfide, sulfur dioxide, and aerosol ions over the Southern Ocean south of Australia, *J. Atmos. Chem., 10,* 341–370, 1990.

Bevington, P., *Data Reduction and Error Analysis for the Physical Sciences*, McGraw-Hill, New-York, 1969.

Capaldo, K.P., and S.N Pandis, Dimethylsulfide chemistry in the remote marine atmosphere: Evaluation and sensitivity analysis of available mechanisms, *J. Geophys. Res., 102,* 23,251–23,267, 1997.

Chameides, W.L., The photochemistry of a marine stratiform cloud, *J. Geophys. Res., 89,* 4739–4755, 1984.

Chameides, W.L. and A.W. Stelson, Aqueous-phase chemical processes in deliquescent sea-salt aerosols: a mechanism that couples the atmospheric cycles of S and sea salt, *J. Geophys. Res., 97,* 20,565–20,580, 1992.

Chin, M., D.J. Jacob, G.M. Gardner, M.S. Foreman-Fowler, and P.A. Spiro, A global three-dimensional model of the tropospheric sulfate, *J. Geophys. Res., 101,* 19,667–19,690, 1996.

Chin, M., R.B. Rood, D.J. Allen, M.O. Andreae, A.M. Thompson, S.-J. Lin, R.M. Atlas, and J.V. Ardizzone, Processes controlling dimethyl sulfide over the ocean: Case studies using a 3-D model driven by assimilated meteorological fields, *J. Geophys. Res., 103,* 8341–8353, 1998.

Cooper, D.J. and E.S. Saltzman, Measurements of atmospheric dimethylsulfide, hydrogen sulfide, and carbon disulfide during GTE/CITE3, *J. Geophys. Res., 98,* 23,397–23,409, 1993.

Davis, D., G. Chen, P. Kasibhatla, A. Jefferson, D. Tanner, F. Eisele, D. Lenschow, W. Neff, and H. Berresheim, DMS oxidation in the Antartic marine boundary layer: Comparison of model simulations and field observations of DMS, DMSO, $DMSO_2$, H_2SO_4(g), MSA(g), and MSA(p), *J. Geophys. Res., 103,* 1657–1678, 1998.

De Bruyn, W.J., T.S. Bates, J.M. Cainey and E.S. Saltzman, Shipboard measurements of dimethyl sulfide and SO_2 southwest of Tasmania during the First Aerosol Characterization Experiment (ACE 1), *J. Geophys. Res., 103,* 16,703–16,711, 1998.

de Leeuw, G., Vertical profiles of giant particles above the sea surface, *Tellus, Ser. B, 38,* 51-61, 1986.

Erickson, D.J. III, S.J. Ghan, and J.E. Penner, Global ocean-to-atmosphere dimethylsulfide flux, *J. Geophys. Res., 95,* 7543–7552, 1990.

Erickson, D.J. III, A stability dependent theory for air-sea gas exchange, *J. Geophys. Res., 98,* 8471–8488, 1993.

Feichter, J., E. Kjellstrom, H. Rodhe, F. Dentener, J. Lelieved, and G.-J. Roelofs, Simulation of the tropospheric sulfur cycle in a global climate model, *Atmos. Environ., 30,* 1693–1707, 1996.

Flossmann, A.I., W.D. Hass, and H.R. Pruppacher, A theoretical study of the wet removal of atmospheric pollutants, I, The redistribution of aerosol particles captured through nucleation and impaction scavenging by growing cloud drop, *J. Atmos. Sci., 42,* 583–606, 1985.

Frew, N.M., The role of organic films in air-sea gas exchange, in *The Sea Surface and Global Change*, edited by P.S. Liss and R.A. Duce, pp. 121–171, Cambridge Univ. Press, New-York, 1997.

Gras, J.L., and G.P. Ayers, Marine aerosol at southern midlatitudes, *J. Geophys. Res., 88,* 10,661–10,666, 1983.

Hoffmann, M.R., and J.G. Calvert, Chemical transformation modules for Eulerian acid deposition models, in *The Aqueous-Phase Chemistry*, pp 3-85, Natl. Cent. for Atmos. Res., Boulder, Col., 1985.

Huebert, B.J., A. Pszenny, B. Blomquist, The ASTEX/MAGE experiment, *J. Geophys. Res., 101,* 4319–4329, 1996.

Huebert, B.J., S.G. Howell, L. Zhuang, J. Heath, M. Litchy, D.J. Wylie, J. Kreidel, S. Coeppicus, and J. Pfeiffer, Filter and impactor measurements of anions and cations during the First Aerosol Characterization Experiment (ACE 1), *J. Geophys. Res., 103,* 16,493–16,509, 1998.

Hynes, A.J., P.H. Wine, and D.H. Semmes, Kinetics and mechanism of OH reactions with organic sulfides, *J. Phys. Chem., 90,* 4148–4156, 1986.

Jacob, D.J., et al., What factors regulate atmospheric aerosol, how have they changed, and how might they change in the future?, in *Aerosol Forcing of Climate*, edited by R.J. Charlson and J. Heitzenberg, pp 183–195, John Wiley, New York, 1995.

Jaenicke, R., *Aerosol-Cloud-Climate Interactions*, pp. 1-32, Academic, San Diego, Calif., 1993.

Jensen, J.B. and R.J. Charlson, On the efficiency of nucleation scavenging, *Tellus, Ser. B, 36,* 367–375, 1984.

Johnson, J.E., and I.S.A Isaksen, Tropospheric ozone chemistry: The impact of cloud chemistry, *J. Atmos. Chem., 16,* 99–122, 1993.

Keene, W.C., R. Sander, A.A.P Pszenny, R. Vogt, P.J. Crutzen, J.N. Galloway, Aerosol pH in the marine boundary layer: A review and model evaluation, *J. Aerosol. Sci., 29,* 339–356, 1998.

Keene, W.C., and D.L. Savoie, The pH of deliquesced sea-salt aerosol in polluted marine air, *Geophys. Res. Lett., 25,* 2181–2184, 1998.

Kreidenweis, S.M., J.E. Penner, F. Yin and J.H. Seinfeld, The effects of dimethylsulfide upon marine aerosol concentrations, *Atmos. Environ., Part A, 25,* 2501–2511, 1991.

Kristament, I.S., J.B. Liley and M.J. Harvey, Aerosol variability in the vertical in the southwest Pacific, *J. Geophys. Res., 98,* 7129–7139, 1993.

Langner, J., and H. Rodhe, A global three-dimensional model of the tropospheric sulfur cycle, *J. Atmos. Chem., 13,* 225–263, 1991.

Lind, J.A., and G.L. Kok, Henry's law determinations for aqueous solutions of hydrogen peroxide, methylhydroperoxide, and peroxyacetic acid, *J. Geophys. Res., 91,* 7889–7895, 1986.

Liss, P.S., and L. Merlivat, Air-sea exchange rates: Introduction and synthesis, in *The Role of Air-Sea Exchange in Geochemical Cycling,* edited by P. Buat-Ménard, pp. 113-127, D. Reidel, Norwell, Mass., 1986.

Lowett, R.F., Quantitative measurements of airborne sea-salt in the North Atlantic, *Tellus, 30,* 372–373, 1978.

Maahs, H.G., Sulfur dioxide/water equilibrium between 0° and 50°: An examination of data at low concentrations, in *Heterogeneous Atmospheric Chemistry*, edited by D.R. Schryer, pp. 187–195, AGU, Washington, D.C., 1983.

Mari, C., K. Suhre, T.S. Bates, J.E. Johnson, R. Rosset, A.R. Bandy, F.L. Eisele, R. Lee Mauldin III, and D.C. Thornton, Physicochemical modeling of the First Aerosol Characterization Experiment (ACE 1) Lagrangian B, 2, DMS emission, transport, and oxidation at the mesoscale, *J. Geophys. Res., 103*, 16,457–16,473, 1998.

Martin, L.R., Kinetic studies of sulfite oxidation in aqueous solution, in *SO_2, NO, NO_2, Oxidation Mechanisms: Atmospheric Considerations*, edited by Calvert, pp. 63-100, Butterworth-Heinemann, Newton, Mass., 1984.

Molenkamp, C.R., and M.M. Bradley, A numerical model of aerosol scavenging, I, Microphysics parameterization, in *Precipitation Scavenging and Atmosphere-Surface Exchange*, vol 1, edited by S.E. Schwartz and W.G.N. Slinn, pp. 575-590, Taylor-Francis, Richland, Wash., 1992.

O'Dowd, C.D., and M.H. Smith, Physico-chemical properties of aerosols over the northeast Atlantic: Evidence for wind speed related submicron sea-salt aerosol production, *J. Geophys. Res., 98*, 1123–1135, 1993.

O'Dowd, C.D., M.H. Smith, I.E. Consterdine, and J.A. Lowe, Marine aerosol, sea salt, and the marine sulphur cycle: A short review, *Atmos. Environ., 31*, 73–80, 1997.

Pandis, S.N., and J.H. Seinfeld, Sensitivity analysis of a chemical mechanism for aqueous-phase atmospheric chemistry, *J. Geophys. Res., 94*, 1105–1126, 1989.

Pham, M., J.-F. Müller, G.P. Brasseur, C. Granier, and G. Mégie, A three-dimensional study of the tropospheric sulfur cycle, *J. Geophys. Res., 100,* 26,061–26,092, 1995.

Pszenny, A.A.P., W.C. Keene, D.J. Jacob, S. Fan, J.R. Maben, M.P. Zetwo, M. Springer-Young, and J.N. Galloway, Evidence of inorganic chlorine gases other than hydrogen chloride in marine surface air, *Geophys. Res. Lett., 20,* 699–702, 1993.

Quinn, P.K., D.J. Coffman, V.N. Kapustin, T.S. Bates, and D.S. Covert, Aerosol optical properties in the marine boundary layer during the First Aerosol Characterization Experiment (ACE 1) and the underlying chemical and physical aerosol properties, *J. Geophys. Res., 103*, 16,547–16,563, 1998.

Russell, L.M., D.H. Lenschow, K.K. Lauren, P.B. Krummel, S.T. Siems, A.R. Bandy, D.C. Thornton, and T.S. Bates, Bidirectional mixing in an ACE 1 marine boundary layer overlain by a second turbulent layer, *J. Geophys. Res., 103*, 16,411–16,432, 1998.

Rutledge, S.A., D.A. Hegg, and P. Hobbs, A numerical model for sulfur and nitrogen scavenging in narrow cold-frontal rainbands, 1, Model description and discussion of microphysical fields, *J. Geophys. Res., 91,* 14,385–14,402, 1986.

Sander, R., and P.J. Crutzen, Model study indicating halogen activation and ozone destruction in polluted air masses transported to sea, *J. Geophys. Res., 101*, 9121–9138, 1996.

Schwartz, S.E., Mass transport considerations pertinent to aqueous phase reactions of gases in liquid-water clouds, in *Multiphase Atmospheric Systems, NATO ASI Ser.*, edited by W. Jaeschke, pp. 415-471, Springer-Verlag, New-York, 1986.

Seinfeld, J.H., and S.N. Pandis, *Atmospheric Chemistry and Physics*, 1326 pp., John Wiley, New-York, 1998.

Sievering, H., J. Boatman, J. Galloway, W. Keene, Y. Kim, M. Luria, and J. Ray, Heterogeneous sulfur conversion in sea-salt aerosol particles: The role of aerosol water content and size distribution, *Atmos. Environ., Part A, 25,* 1479–1487, 1991.

Sievering, H., J. Boatman, E. Gorman, Y. Kim, L. Anderson, G. Ennis, M. Luria and S. Pandis, Removal of sulphur from the marine boundary layer by ozone oxidation in sea-salt aerosols, *Nature, 360,* 571–573, 1992.

Sievering, H., E. Gorman, T. Ley, A. Pszenny, M. Springer-Young, J. Boartman, Y. Kim, C. Nagamoto and D. Wellman, Ozone oxidation of sulfur in sea-salt aerosol particles during the Azores Marine Aerosol and Gas Exchange experiment, *J. Geophys. Res., 100,* 23,075–23,081, 1995.

Sievering, H., B. Lerner, J. Slavich, J. Anderson, M. Posfai, and J. Cainey, O_3 oxidation of SO_2 in sea-salt aerosol water: Size distribution of non-sea-salt sulfate during ACE 1, *J. Geophys. Res.*, , this issue.

Suhre, K., M.O. Andreae, and R. Rosset, Biogenic sulfur emissions and aerosols over the tropical South Atlantic, 2, One-dimensional simulation of sulfur chemistry in the marine boundary layer, *J. Geophys. Res., 100*, 11,323–11,334, 1995.

Suhre, K., et al., Physico-chemical modeling of the First Aerosol Characterization Experiment (ACE 1) Lagrangian B, 1, A moving column approach, *J. Geophys. Res., 103,* 16,433–16,455, 1998.

Toumi, R., BrO as a sink for dimethylsulphide in the marine atmosphere, *Geophys. Res. Lett.*, 21, 117–120, 1994.

Vogt, R., P.J. Crutzen, and R. Sander, A mechanism for halogen release from sea-salt aerosol in the remote marine boundary layer, *Nature, 383*, 327–330, 1996.

Wanninkhof, R., Relationship between wind speed and gas exchange over the ocean, *J. Geophys. Res., 97*, 7373–7382, 1992.

Wesely, M., Parameterization of surface resistances to gaseous dry deposition in regional-scale numerical models, *Atmos. Environ., 23*, 1293–1304, 1989.

Winkler, P., Relations between aerosol acidity and ion balance, in *Chemistry of Multiphase Atmospheric Systems, NATO ASI Ser.,* vol. 6G, edited by W. Jaeschke, pp. 269-298, Springer-Verlag, New York, 1986.

Woodcock, A.H., Salt nuclei in marine air as a function of attitude and wind force, *J. Meteorol., 10*, 362-371, 1953.

Yvon, S.A., E.S. Saltzman, D.J. Cooper, T.S. Bates, and A.M. Thompson, Atmospheric dimethylsulfide cycling at a tropical South Pacific station (12°S, 135°W): A comparison of field and model results, *J. Geophys. Res., 101,* 6899–6910, 1996.

A. R. Bandy and D. C. Thornton, Department of Chemistry, Drexel University, Philadelphia, PA 19104.

T. S. Bates, Pacific Marine Environmental Laboratory, NOAA, 7600 Sand Point Way NE, Seattle, WA 98115.

S. Businger, Department of Meteorology, University of Hawaii at Manoa, Honolulu, HI 96822.

B. J. Huebert, Department of Oceanography, School of Ocean and Earth Science and Technology, University of Hawaii at Manoa, 1000 Pope Road, Honolulu, HI 96822.

C. Mari, R. Rosset and K. Suhre, Laboratoire d'Aérologie, UMR 5560 CNRS/Université Paul Sabatier, 31400 Toulouse, France. (e-mail: marc@aero.obs-mip.fr)

(Received October 5, 1998; revised January 4, 1999; accepted January 11, 1999.)